




## Article

# Controlled Laboratory Generation of Atmospheric Black Carbon Using Laser Excitation-Based Soot Generator: From Basic Principles to Application Perspectives: A Review

Tibor Ajtai <sup>1,\*</sup>, Attila Kohut <sup>1</sup> , Péter Raffai <sup>1</sup> , Gábor Szabó <sup>1</sup> and Zoltán Bozóki <sup>1,2</sup> <sup>1</sup> Department of Optics and Quantum Electronics, University of Szeged, H-6720 Szeged, Hungary<sup>2</sup> ELKH-SZTE Research Group for Photoacoustic Monitoring of Environmental Processes, Dóm tér 9, H-6720 Szeged, Hungary

\* Correspondence: ajtai@titan.physx.u-szeged.hu

**Abstract:** The mimicking of atmospheric soot with versatile chemophysical properties is a critical issue in many applications, starting from instrument calibration, through producing aerosol standards for academic research, and ending with the reduction of uncertainties associated to carbonaceous particulate matter in the atmosphere, just to name a few. The present study deals with laser ablation as a novel and interesting technique for the generation of soot with high elementary carbon (EC) content with microphysical features similar to diesel or atmospheric soot and for modelling biomass emission under well-controlled laboratory conditions. The operation of the laser-excitation-based soot generator and the characteristics of the produced particles are compared to the most widely used techniques like flame, spark discharge generators, and real combustion soot originating from diesel- and aircraft engines or from field measurement. The comparison shows that significant differences in the physicochemical features exist between the real combustion soot and the soot originating from different excitation mechanisms. Moreover, the soot produced by different techniques shown also significant differences. However, due to some inherent and favorable attributes of the laser ablation technique—such as the possibility of the independent variation of physical characteristics of the generated soot particles—the potential for modelling biomass burning or to produce soot particles even in the accumulation mode makes it a useful tool in many cases.

**Keywords:** laser ablation; atmospheric soot; spark discharge; combustion flame



**Citation:** Ajtai, T.; Kohut, A.; Raffai, P.; Szabó, G.; Bozóki, Z. Controlled Laboratory Generation of Atmospheric Black Carbon Using Laser Excitation-Based Soot Generator: From Basic Principles to Application Perspectives: A Review. *Atmosphere* **2022**, *13*, 1366. <https://doi.org/10.3390/atmos13091366>

Academic Editors: Sandra Mogo, Edith Rodriguez, Natalia Prats and Boris Barja

Received: 28 June 2022

Accepted: 18 August 2022

Published: 26 August 2022

**Publisher's Note:** MDPI stays neutral with regard to jurisdictional claims in published maps and institutional affiliations.



**Copyright:** © 2022 by the authors. Licensee MDPI, Basel, Switzerland. This article is an open access article distributed under the terms and conditions of the Creative Commons Attribution (CC BY) license (<https://creativecommons.org/licenses/by/4.0/>).

## 1. Introduction

Interest in atmospheric soot has been gradually increasing in many contexts, starting from its effects on climate, through its adverse health relevance, to its regulation aspects and mitigation strategy [1–5]. One of the major contributors to the carbon cycle is CPM (Carbonaceous Particulate Matter) which is the second most important climate-related [2] and one of the most harmful atmospheric constituents [6]. CPM has complex and versatile physicochemical properties, which—during its lifetime in the atmosphere—are changing dynamically. First, the particle evolution progresses through nucleation, coagulation, and aggregation processes in the combustion zone [7]. Then, the source-specific emission characteristics of CPM develop nearby the emission source. Moving away from the emission source, the physical and chemical aging masks the initial emission characteristics. The observed apparent feature of CPM depends on the physicochemical reactions in the atmosphere, the on spot meteorological conditions, its lifetime, and its trajectory [8]. To reduce the uncertainties associated with CPM, the laboratory-controlled generation of soot fractal aggregates and imitation of atmospheric processes are deemed essential [9,10]. However, the measured quantities generally used to characterize CPM depend not only on the initial burning conditions or fuel types but also on diverse environmental factors. Therefore, it is highly desired if the applied generation method can provide not only a soot

surrogate with a definite and complex set of parameters but that parameters can also be modified independently from each other. A further difficulty is that the atmospheric soot has operative definitions, which means that all definitions used in the scientific community are associated with a particular quantity of the respective carbonaceous fraction or with the applied methods. The problems referring to the confusion in terms and definitions are described in detail elsewhere [9]. Therefore, the generation of a soot aerosol standard for instrument calibration and validation is an actual and important issue in atmospheric science today. There are many different methods of producing soot particles for both scientific and industrial usage. However, two widely used approaches for the generation of carbonaceous particulate dispersed in a gas matrix are the spark discharge and the diffusion flame methods [11–16]. Although both of them produce CPM with high stability and reproducibility even in a long-term operation, they only partially fulfill the above-mentioned requirements. So, introducing alternatives for soot particle production is a relevant and actual scientific issue. In 2015, for example, a demonstrative study for controlled generation of soot nanofractal aggregates based on the laser excitation of high purity graphite target was published [17].

In the present study, operation and particle characteristics of laser excitation-based soot generation are compared to the most widespread alternatives, such as soot flaming and spark discharge generation. We carried out a comprehensive analysis of soot evolution tendencies and the characteristic performances of the produced particles using different excitation approaches. Finally, we also compare the physicochemical features of the produced aerosols in application perspectives.

## 2. Soot Formation Using Different Excitation Mechanisms and Precursor Types

### 2.1. Flames

Through some cross-talking, on the basis of Rafinesque postulate: soot particles may be formed in the great chemical laboratory in our atmosphere [18]. Soot is a byproduct of incomplete combustion having versatile physicochemical features. The natural or refined fuels may have hundreds of different composites, therefore detailed and fundamental modelling of soot formation in combustion is difficult. Soot formation in combustion is a complex process including a number of chemical and physical steps (Figure 1). Although it is complicated and depends on the type of fuel and flaming conditions, there is a general description of the reaction path that leads to the formation of soot. Initially, at high temperature, the chain reactions of resonance-stabilized radicals and hydrocarbons resulted in initial polyaromatic hydrocarbons (PAH) in the pyrolysis zone. Then molecular growth and soot precursor formation takes places. This is followed by the dimerization and oligomer formation of PAHs [19]. The next step is the soot inception, where the nascent soot evolves in a gas to particle conversion (so-called nucleation) [20]. The soot nuclei then continuously grow via coagulation process which results in an onion like graphitic molecule structure that retains its spherical shape. Finally, the aggregation of primary particles and the further graphitization of those take place, resulting in fractal geometry of the evolved CPM. In the soot formation process the chemical and physical properties change dynamically. The C/H ratio and the density continuously increase from around 1 (nascent soot) to around 10–20 (fractal aggregates) and from around 1.3 g/cm<sup>3</sup> (nascent soot) to about 1.8–2 g/cm<sup>3</sup> (fractal aggregates), respectively [21]. The surface reactivity is decreased, while the optical properties also dramatically change through the evolution of soot particles [22].

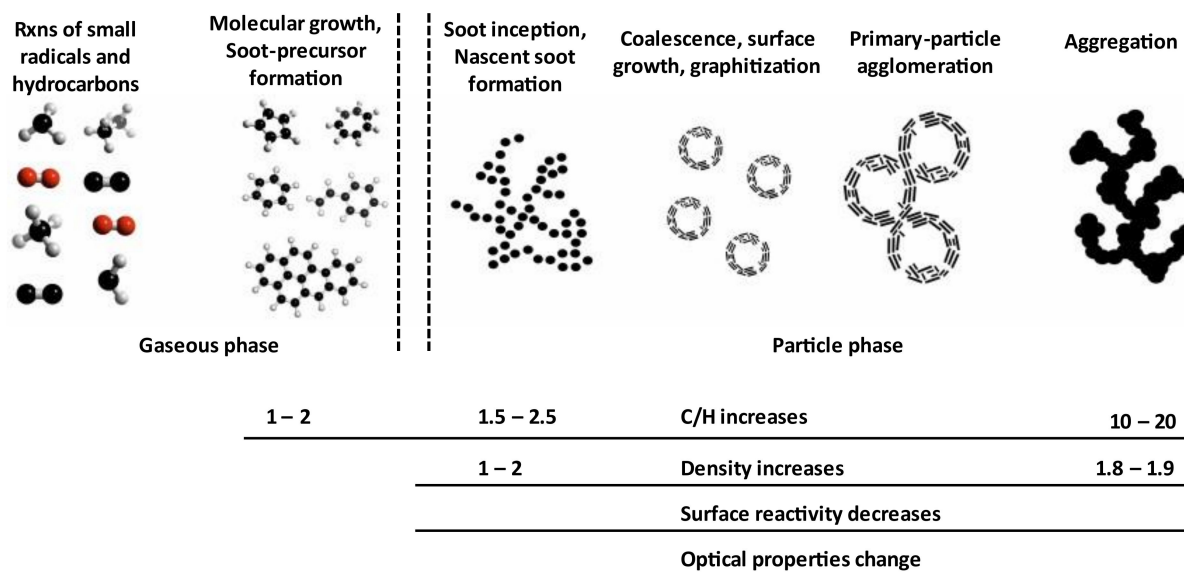
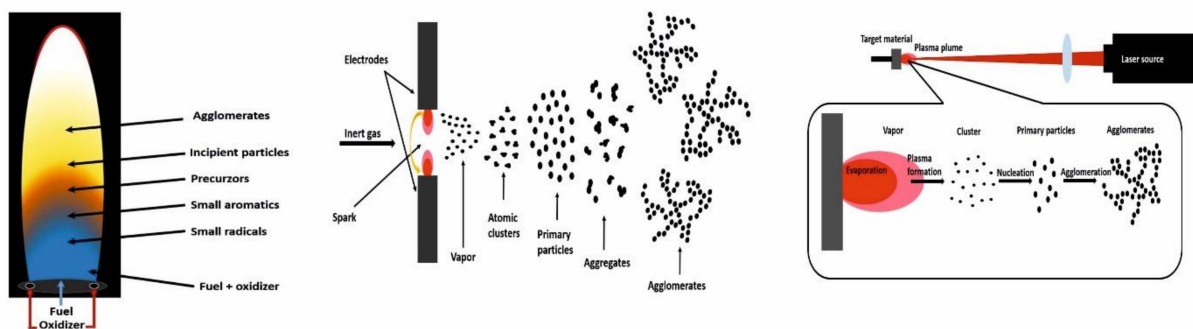


Figure 1. The soot formation and its characteristics.

The evolution of soot in the combustion process is simulated in laboratory circumstances using a mixture of reduced fuel composites and an oxidant gas under various instrument configurations. The controlled, laboratory generation of soot in flames is carried out using the mixture of a hydrocarbon compound (such as propane) and synthetic air in versatile and defined experimental configurations, such as per-mixed flame, normal, and inverse co-annular or counter flowing diffusion. The soot evolution is mainly influenced by the fuel structure but also affected by the applied experimental configuration. Irrespectively of the applied diffusion flame, the soot inception occurs around 1400 K, while particle burnout ceases at about 1300 K. Although the soot evolution is follows the same steps described above, some configuration-dependent technical details have to be mentioned here (Figure 2, left). Briefly, in combustion flame, soot particles are formed due to the pyrolysis of hydrocarbons inside the combustion zone. The combustion zone is heated by various oxidation reactions inside the flame. The defined flame construction ensures the symmetrical temperature and oxidation distribution geometry. Particle inception and growth takes place along the vertical axis of the flame. Molecular growth and soot precursor formation takes places at the flame front. At low flame position soot nuclei form and grow further through coagulation and aggregation towards the higher flame position. However, due to the oxidation layer, at the surface of the flame few or no soot particles survive, as they burn up when crossing through this oxidation layer [23]. The soot particle can only escape from the flame by quenching the combustion process at a certain height of the flame. Quenching interrupts the chemical reaction and “freezes” the soot particle at a given state of its evolution that corresponds to the moment in which the combustion process is interrupted. Therefore, varying the vertical position of quenching, the characteristic properties of the soot fractal aggregates can be altered. Alternatively, varying the flow of the fuel gas and the oxidizing air the height of the flame can be modified, thereby the given size distribution can also be influenced at a given quenching position as well.



**Figure 2.** The soot tendency under different excitations mechanism: flame (left), spark discharge (center), laser ablation (right).

### 2.2. Spark Discharges

For producing pure elementary carbon (EC)—or in optical terminology black carbon (BC)—under well-controlled laboratory circumstances, the spark discharge generator (SDG) is a widely accepted approach in the field of environmental research (PALAS; GFG series) [24,25]. In this technique several microsecond-long, high-voltage, high-current electric discharges are produced repetitively between two solid electrodes, providing sufficiently high temperature to evaporate a relatively small fraction of the electrode material (Figure 2, center). The repetitive sparking is maintained in a flowing—usually inert—gas under atmospheric pressure. The vapor plume generated during sparking expands rapidly and characterized by high cooling rates [26]. Due to supersaturation occurring in the plume, vapor to particle transition takes place and soot nuclei can be formed [27]. The soot nuclei can then coagulate, resulting in primary spherical particles, followed by the aggregation and agglomeration of the primary particles as the final step. When high purity graphite electrodes are used, the chemical composition of the generated particles differs from the chemical composition of the real combustion soot aerosol, but in terms of physical properties they are the facsimile of ambient CPM. Unlike combustion particles, which contain hydrocarbons and a broad selection of contaminants due to the more complex chemical composition of the fuel and the more elaborate combustion process, SDG-based particles have carbon-like molecule structure with little or no contamination. However, this depends on the exact experimental conditions, since the generated aerosol purity primarily depends on the purity of the electrodes, the carrier gas, and the composition of the generator chamber. As an example to the significance of the electrode purity, one can note that standard graphite electrodes contain approximately 20  $\mu\text{g/g}$  ash, while low-ash-content electrodes contain less than 2  $\mu\text{g/g}$  [28]. Moreover, organics evaporating from the walls and tubing of the generator can also play a major role in defining the purity of the generated carbonaceous particles. It was shown that the weight percent of organic volatile materials in SDG-generated carbon particles can be reduced from ca. 25% to 6% by employing ceramic and stainless-steel components, instead of polymers [29]. By varying the operational parameters, such as flow rate, spark energy, and spark repetition rate, different microphysical properties of the soot aerosol can be mimicked both on the primary particle and on the agglomerate level [27]. Increasing the flow rate, the characteristic size of the agglomerates can be affected. The higher the flow rate, the smaller the characteristic size of the emitted carbon particles, while increasing the spark repetition rate will increase both the characteristic size and the number-concentration of the particles [24]. It should be noted that the variation of the different experimental parameters usually has a coupled effect on different aerosol properties, which has to be taken into account during the application of the technique.

### 2.3. Laser Ablation

As an alternative to the more common techniques briefly introduced above, a novel methodology based on the laser excitation of monolithic graphite material for producing pure elemental carbon with high EC content or to mimic real biomass emission process

was introduced recently [17]. Pulsed laser ablation is a well-established method for solid surface modification or nanostructure synthesis. In this approach, interaction between a laser pulse and the solid target leads to the formation of nano particulates (Figure 2, right). For nanosecond or longer laser pulses the ablation process is often described by a thermal evaporation model. However, in case of ultra-short laser excitation additional non-equilibrium processes, such as explosive boiling, spallation, spinodal decomposition, etc., take place [30–32]. In the thermal evaporation approach—nanosecond regime—the laser-initiated plasma is heated due to the absorption of laser energy through inverse Bremsstrahlung, and the duration of material removal from the target correlates with the temporal width of the laser pulse. Depending on laser wavelengths and characteristic plasma parameters, the temperature of the generated plasma rises up to ~10,000 K. Since both techniques are based on the atomization of a bulk target material involving plasma formation, it is worth taking a closer look on the similarities and differences between the laser- and the spark-based ablation. In SDGs the so-called Townsend avalanche multiplication occurs due to the high voltage in the interelectrode gap, which results in the formation of a conducting plasma column and the erosion and local evaporation of the electrodes [33]. The peak gas temperature in an SDG plasma is ca. 20,000 K, and the evaporation duration falls typically into the  $\mu\text{s}$  time domain [34]. Therefore, in terms of plasma formation, the main differences between laser ablation (LA) and spark ablation are the time scale of excitation and the way of energy transfer to the target material (i.e., photons in LA and charge carriers in an SDG). While SDGs usually operate at atmospheric pressure, the plasma expansion in LA strongly depends on the pressure and other conditions of the ambient gas. When the LA process is taking place in vacuum, collisional quenching occurs; therefore, initial plume composition is not affected by the plume expansion. When LA process is taking place in ambient air or in high pressure buffer gas, the plasma plume is strongly compressed and its expansion becomes slower. As a result, abundant number of collisions are taking place triggering the process of nucleation. Regardless of the excitation method, after plasma formation the tendency of soot evolution is followed by nucleation, coagulation, and aggregation processes resulting in fractal-like soot aggregates with a graphitic or turbostratic molecular structure. Nucleation can be classified as a gas to aerosol transition, which is dominantly a chemical process. However, particle evolution via coagulation and aggregation are functionally physical and competitive processes. The ratio of coalescence and collision times determine their relative dominance. When  $\tau_{\text{coalescence}} > \tau_{\text{collision}}$  spherical particle, while when  $\tau_{\text{coalescence}} < \tau_{\text{collision}}$  fractal aggregates form. Briefly, if the particle temperature is close to the temperature of the surrounding gas the particles stick to each other when they collide. In case of coalescence, the total surface energy decreases if the time of collision is smaller than the time that is needed to cool the initial particles down to gas temperature. The temperature of the colliding particles is increased by the collision allowing coalescence to be more complete. If the coalescence is complete, new spherical particles form from the initial ones. If the coalescence is not complete, agglomerates can occur. With rapid cooling of particles, the aggregation process becomes dominant as the time between the collisions of the initial particles becomes longer than the time taken to cool down the particles. This occurs inherently when the plasma expands and the carrier gas removes the particles from the active zone. In case of SDG, this happens further away from the interelectrode gap, while in case of LA far from the exposed target surface in the chamber. With LA, the microphysical properties of the generated soot particles can be affected by the flow rate and the composition of the carrier gas as well as the applied laser wavelength and its fluence. Similarly to that of the SDG products, the LA-produced soot aerosol is different from real ambient soot particles in chemical aspects but mimics their microphysical properties well. Using high purity carbon standard, it creates high purity EC or BC (black carbon) particles. The laser excitation parameters can be more strictly controlled than those of the spark discharge; therefore, the conditions of particle generation are better controlled in the LA than in SDGs. Furthermore, the less strict restrictions on the carrier gas and target material in the LA method provide more flexibility in practical



applications. In the LA method even biomass or residential coal aerosol can be used as a fuel; therefore, it can provide a novel opportunity to model the real combustion phenomena under well controlled laboratory circumstances [8,35–37]. However, one of the drawbacks of the LA technique is the relatively small yield and that upscaling is challenging with multiple laser beam excitation.

### 3. Experimental Set-Ups for Soot Generation with Different Mechanisms

#### 3.1. Flames

Due to its significant importance on environment and health, great scientific and technological efforts have been devoted to investigating soot formation mechanisms and understand the different parameters and boundary conditions that determine the properties of the resulting particles and the related phenomena. As a natural consequence, experimental methods are also developed for the controlled generation and investigation of soot, the most prominent approach of which utilizes flames. Various configurations of controlled flames—including per-mixed flame, normal, and invers co-annular or counter flowing—are available for mimicking ambient soot under controlled measurement conditions. Providing a comprehensive description of the available experimental methods and the corresponding peculiarities of the generated soot particles is far beyond the scope of the present paper, but the readers should refer to various sources on this broad topic [7,38–41]. Here, for the sake of our discussion on LA-based soot generation we only briefly describe one of the most widely used configurations, the so-called co-flow diffusion flame (Figure 3, left.), which is also the basis of the well-established commercial instrument for soot production, the so-called Combustion Aerosol Standard (CAST) by the company Jing ([www.sootgenerator.com](http://www.sootgenerator.com) accessed on 2 May 2022). In this configuration, the burner consists of a coaxial inner tube containing the gaseous fuel stream and an outer tube delivering particle-free synthetic air stream. At the flame front, where the fuel and the oxidizer layer are mixed the pyrolysis and soot formation is started. The configuration of this burner enables the escape of the evolved soot particles from the flame without contact with oxygen. At higher positions of the flame quenching gas is mixed in to prevent further combustion processes and to stabilize the particle properties. For further dilution synthetic air is mixed with the quenching gas. There are numerous ways to modify the physicochemical properties of the generated soot aerosol in this approach. Soot concentration and properties can be varied by modifying the flow rate of fuel, oxidant, quenching ( $N_2$ ), and dilution gas [42,43]. Lean and rich-fuel conditions can also be modeled by mixing inert gas with the applied fuel. These settings make it possible to produce soot particles with varying physicochemical properties [12]. However, modifying any operational parameters of the burner can lead to change in many microphysical and chemical parameters of the generated aerosol sample. The independent variation of the characteristic parameters of the generated soot particles cannot be achieved in this configuration.

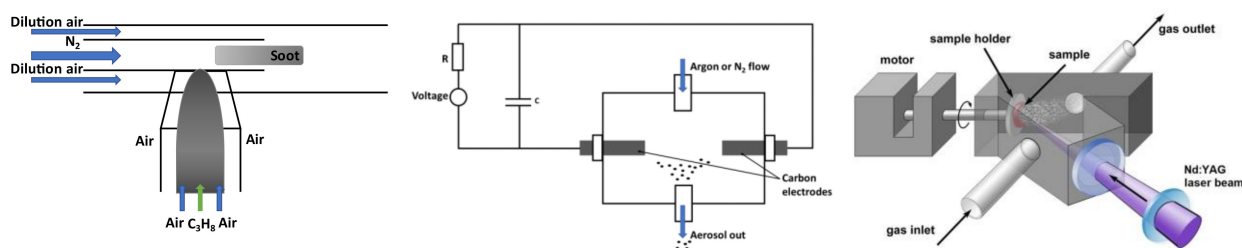


**Figure 3.** The schematic of the experimental set-up of soot generator using different excitations: sooting flame (left), spark discharge (center), laser ablation (right).

#### 3.2. Spark Discharges

The experimental set-up of the SDG consists of two major parts: a chamber to house the electrodes ensuring proper gap between them and the electric circuit to control the

generation of spark discharge (Figure 3, center). SDGs are operated in a controlled, flowing gaseous environment at (around) atmospheric pressure. Nitrogen and argon are commonly used as carrier gas. They do not cause significant change in the density of the exhaust gas. The general design of SDGs for laboratories producing atmospheric soot consists of two high purity carbon electrodes separated by a defined gap. The monolithic graphite electrodes are usually cylindrical and are fixed in the chamber in an end-toward-end configuration with a defined gap between them. By charging the shunted capacitor, high voltage is applied across the gap. When the electric field between the electrodes is high enough, the accelerated cations and electrons gain sufficient energy to further ionize the surrounding gas molecules. This gives rise to electron avalanche and forms a conductive plasma channel. The energy transfer between the spark and the carbon electrodes leads to erosion and evaporation of the exposed electrode surfaces. After the capacitor is fully discharged the plasma ceases and the charging cycle starts over, until the voltage is high enough to initiate a spark discharge again. These charging–discharging cycles are continuously repeated, resulting in a steady repetitive sparking, each of them ripping a tiny amount of graphite off the electrodes. In the vaporized plasma state the initial formation of soot nuclei takes place. Then the soot nuclei—due to their high number concentration—undergo collision-induced coagulation, while the expansion (and therefore cooling) of the plasma allows the aggregation process to start. Due to the constant sparkover voltage, the energy converted in each spark remains constant. The constant energy of each individual spark provides stable size distribution and concentration of soot particles [44]. The mass of the generated soot aerosol assembly can be easily adjusted and controlled by spark repetition rate (or spark frequency) within a wide range [24]. It should be noted that the prolonged erosion of the graphite target at a given frequency modifies the gap between the electrodes, which imposes a limitation on the stability of the yield. To avoid the decrement in concentration and to increase the reproducibility factor, the readjustment of the gap between the graphite electrodes is deemed essential. An important advantage of the spark-based excitation is the potential in scaling up the particle yield, since using more devices in parallel makes it possible to further increase the concentration [45]. If the opposite is required, synthetic air flow as dilution gas can be used outside the chamber to decrease the concentration of the output aerosol [24]. Due to the high purity of the monolithic carbon electrodes the generated aerosol assembly can mimic the microphysical properties of pure elemental carbon structures or diesel soot with only moderate limitations (see in detail later).

### 3.3. Laser Ablation

Laser excitation can also be used to generate an aerosol standard or to produce real carbon aerosols under well-controlled laboratory circumstances. The principal design of the LA setup consists of two parts: a pulsed laser as a light source and an ablation chamber containing the solid target (Figure 3, right). The operating parameters of the laser are the laser wavelength, the pulse duration and the laser pulse energy per unit area (fluence). In addition to the laser parameters, the thermo-optical properties of the targeted fuel strongly affect the physicochemical properties of the generated soot aerosol assembly too. There are many experimental and theoretical studies discussing the formation of soot produced by the ablation technique. Using nanosecond or longer laser pulses nucleation, condensation, coagulation, and aggregation are the major physical processes. The nanosecond KrF excimer laser with operational wavelength and pulse duration of 248 nm and 18 ns, respectively, was first used to demonstrate the applicability of the laser ablation method to surrogate atmospheric soot under laboratory-controlled circumstances [17]. In this configuration, the laser fluence and, therefore, the laser power should be kept constant to ensure the constant yield throughout the measurement period. For this purpose, to continuously monitor the pulse energy a quartz plate is placed into the path of the laser beam which serves as an energy coupler, reflecting 4% of the total laser energy onto the surface of the energy meter. A high purity monolithic graphite disc (with diameter and thickness of 3 cm and 5 cm, respectively) is used as a target material. The laser energy which is needed for triggering

soot evolution depends on the applied wavelength, the laser power, and the thermo-optical properties of graphite. Under a threshold value the applied laser energy is not enough for soot production. Above the threshold level the photon energy is absorbed by the graphite target, which leads to its erosion and evaporation. By focusing the laser beam, energy density (fluence) can be maximized. The focused laser beam rips tiny amount of material from the surface creating a tight and deep ablation crater with width in the order of  $10^{-7}$  m; therefore, a subsequent pulse on the same spot results in a smaller yield from that area. To improve the concentration stability of the generated particle assembly, the graphite target is placed onto a rotating sample holder and the angular speed of the rotation is fitted to the repetition rate of the laser and the irradiated area of the target. This way uniform etching can be ensured. This configuration ensures a stable concentration yield over several hours. The smoothing of the graphite disc surface from time to time is deemed essential to ensure high degree of reproducibility. The focused laser beam is lead into the chamber through a fused silica window at an angle of  $45^\circ$  with respect to the surface of the target material. The chamber is designed to minimize size-dependent particle losses. The inlet and outlet pipes are installed into the opposite sides of the chamber ensuring a straight gas flow through the ablation module. The mass concentration of the generated aerosol can be increased with increasing the repetition rate of the pulses. In LA, the laser pulse energy is converted into heat on the targeted sample to trigger the evolution of soot. The applied laser fluence typically falls between 0.5 and  $3.0 \text{ J/cm}^2$ . The radius of the irradiated area is generally in the order of mm. From a practical point of view, an important advantage of LA is the flexibility of the target material. Unlike in SDGs, where the material selection is limited to conductive materials, which can be machined to cylindrical electrodes, in case of LA, besides the monolithic graphite, real carbonaceous fuels including biomass or residential coal samples can also be ablated. A further advantage of LA is its green character, namely that the generated nanoparticles are almost unaffected chemically, which can be achieved by using high purity monolithic graphite fuel and inert  $\text{N}_2$  puffer gas or high purity synthetic air. Moreover, in LA, there is no restriction for the background gases, one can either use inert or reactive ones.

#### 4. Characteristic Performance of Soot Particles Using Different Excitations

Many excellent papers have demonstrated the applicability of different techniques for modeling ambient soot under well-controlled laboratory circumstances [12,17,44,46–48]. The characteristic performance of the generated soot using sooting flames, SDG, and LA methods are summarized in Table 1. The combustion flame using the fuel gas standard in a controlled arrangement is a versatile tool for mimicking different physicochemical properties of carbonaceous particulate matter in the atmosphere. Varying the operative parameters, including gas flow rates, and mixing and quenching gas positions makes it possible to imitate real combustion phenomena associated with different conditions of combustion. These settings allow us to vary the size distribution, the optical properties, chemical reflectivity, and also the soot chemistry. However, if even one operative parameter is changed, both the physical and the chemical characteristics of the yield are modified simultaneously. Therefore, this method is capable of producing a model soot with specific and complex set of parameters but is not able to modify the relevant properties of it independently from each other. By mixing the fuel with inert gas, the lean- and the rich-fuel conditions of combustion can be simulated. The flame chemistry is defined through the overall fuel-to-air or molar C/O ratio. The flame can be categorized as rich-fuel when  $\text{C/O} > 3$  or as lean-fuel when  $\text{C/O} < 3$ . The C/O ratio can also be varied by mixing the fuel directly with air (premixed option). Using different C/O ratios, unimodal size distribution with GMD (Geometric Mean Diameter) of 20 nm to 300 nm can be produced. The largest GMD value associates to the near stoichiometric condition ( $\text{C/O} \sim 0.3$ ), while both lean and rich-fuel conditions provide particles of smaller GMD [12]. The flame chemistry affects the chemical and spectral characteristics of the generated carbonaceous particles, which is determined through chemical refractivity (EC/OC or EC/TC ratio), or via an



optical approach where the BC/BrC ratio is quantified through the slope of wavelength dependency of the absorption spectra (AAE—Absorption Ångström Exponent) [49]. The extinction spectra of soot generated by diffusion flame is thoroughly investigated in the climate relevant wavelength domain too [50,51]. Modifying the C/O ratio from very fuel-rich (C/O = 1) to slightly fuel-lean conditions increases GMD values from 40 nm to 300 nm and EC content from about 20% to 80%, as well as decreasing AAE from around 9 to 1 [11,12,52,53]. Similarly, at slightly fuel-rich condition, tuning the characteristic size of the generated particles by diluting the fuel gas with N<sub>2</sub> resulted in the following changes in particle characteristics: the higher the dilution factor, the smaller the GMD (100 nm to 300 nm) and the higher the AAE (1–3.5) and OC/TC ratio (10–50%) of the particles [11]. The morphology and the microstructure of the generated soot particles is fractal-like, consisting primary spherical particles with the diameter of about 5–20 nm with varied fractal dimensions from about 1.7 to 2.3 (Table 1). The different configurations of flames are often used to simulate soot originated from real-world sources (i.e., diesel or aircraft engines), to calibrate or validate instruments, or to study real atmospheric processes. Carbonaceous particulate assemblies emitted by diesel or aircraft engines display various physiochemical features. Substitution particulate matter, not only the physical characteristics but also the chemical composition and optical properties of which are similar to those of soot particles is deemed essential. The characteristic properties of soot generated by a specific flame set-up (i.e., miniCAST BC, [www.generators.com](http://www.generators.com) accessed by 2 of May 2022) operating under various measurement conditions are summarized in Table 1. For comparison, diesel- and aircraft exhaust and some relevant field measurement data are also shown in Table 1. In order to simulate diesel soot with high EC content around or below 100 nm characteristic size, the miniCAST BC can be operated either in diffusion flame mode at fuel-lean condition or premixed flame mode around the stoichiometric condition (C/O~0.3), where soot of high EC and low AAE can be produced. In contrast, the surrogate of aircraft soot should be done with high OC content at fuel-rich setting. If the nonvolatile aircraft emission with lower OC content is to be simulated, the operation mode of fuel-lean measurement condition should be used [12]. Similarly, the flame can be used for simulating the multifarious physicochemical nature of ambient soot originating from different sources (Table 1). However, it is worth to note, that the mixing state of the generated soot particles differs from that of real soot particles. In summary, the diffusion flames technique extends our capabilities to simulate real soot aerosol with versatile physicochemical features.

In the past decades, many studies have investigated the distinct characteristics of the SDG-based method [24,38,54,55]. The method has been standardized in the technical rule VDI 3497 (VDI 3491 Blatt 4:2018-03 Technical rule). The company PALAS built the first commercial SDG instrument (Palas-GFG-1000) for producing high quality soot standard with high concentration stability and reproducibility. Currently, the improved version of the PALAS GFG series is the most widespread instrument for modeling the physical properties of atmospheric soot. By using GFG with carbon electrodes the soot is formed from elementary carbon particles; thus, they are still a good standard for the physical properties of combustion products. They can generate EC (BC) aerosol in the size domain of real combustion-produced aerosol. Therefore, the GFG-produced soot aerosol is generally used to surrogate aerosols with high EC content. The major application areas of SDG are the production of soot aerosol standards for tests and to calibrate measurement devices, reactivity studies to evaluate after-treatment devices and their regeneration strategies, and for simulating the physical properties of real carbonaceous aerosol [14,52,56,57]. Compared to flames, the major advantages of the SDG approach are its simplicity and easy and contamination-free operation. The set-up allows for the decoupling of the spark energy (determined by the capacity and voltage but independent from the electrode distance) from the repetition rate of the discharge. The size distribution then becomes mainly independent of the shape and the distance of the electrodes. The mass yield per pulse can be regulated by the pulse energy through the capacitance and the applied voltage. By using different spark frequencies and flow rates of argon or nitrogen gases, soot aerosol with

different GMD values can be produced even in the 25 nm to 200 nm range [24,44,50,51] (Table 1). The morphology and the microstructure of the SDG-generated soot particles were also investigated in many studies (Table 1). The carbon fractal nanoaggregates consist of primary particles in the size domain of 5–10 nm, while their fractal dimension falls between 1.7 and 2.3 [8]. The effective density of the GFG soot is decreasing at higher sizes from around 1.5 close to 0 values. Obviously, the higher particle production rate resulted in a lower effective density, due to the higher degree of agglomeration. The GFG-produced soot particles possess heterogeneous and functionalized microstructure; however, the microstructure of GFG soot differs substantially from that of pure EC or diesel soot [58]. GFG soot has a high number of defects and deviations from perfect elemental carbon structures, as it has a spherically symmetric onion-like arrangement resulting in increased surface functionalization [58]. An increase of structural order and decrease of chemical heterogeneity of GFG soot are found upon oxidation. The spectral response of GFG soot was also investigated and compared to diesel emissions. It was found that the mass-specific absorption cross section of GFG soot is almost halved compared to that of diesel soot in the climatically-relevant near-infrared to UV wavelength region [46]. The AAE value of GFG and diesel soot was compared and determined [46]. The AAE of diesel emission was found to be much smaller than that of GFG soot (Table 1). The AAE value of GFG soot is very similar to that of residential coal or ambient soot measured in urban circumstances even in the winter season [34,35]. The primary particles of GFG soot (5–8 nm) is substantially smaller than that of real diesel soot. Due to the relatively low fractal dimension (1.7–2.1), every single primary particle acts independently and dominates light scattering. Thus, considering the spectral responses, GFG soot is not a good proxy for modeling atmospheric soot and real combustion soot particles [58]. This should be of primary concern when calibrating soot sensors based on the scattering, extinction, and absorption of soot particles.

The characteristic performance of LA-produced soot using high purity monolithic graphite target and nanosecond laser excitation operated at 248 nm wavelength were determined under various operational conditions [17]. The soot particle yield was increased by increasing the laser fluence from 0.5 J/cm<sup>2</sup> to 2.5 J/cm<sup>2</sup> in this configuration. At low fluence (below 0.9 J/cm<sup>2</sup>) the mass concentration of the generated particles was found to be almost independent from the applied fluence. Above 0.9 J/cm<sup>2</sup> fluence, mass concentration of the generated soot particles increased roughly linearly with fluence. A simple but plausible explanation of this behavior is that at low fluences, the excitation causes fragmentation on the irradiated surface, which is primarily supposed to be a surface phenomenon and independent of the applied fluence. However, at higher fluences, the yield of the produced soot assembly is proportional to the whole ablated volume determined by the penetration depth of the laser pulses [17]. Therefore, in this regime, the yield of the generated aerosol is scaled by the laser fluence. The LA-produced size distributions show differences at different fluences. At fluences of about 0.7 J/cm<sup>2</sup>, the LA soot assembly dominantly comprise a high number of primary particles of spherical geometry with various sizes in the range of about 10 nm to 22 nm. The number of aggregates is negligible. In the low fluence regime, either the number of primary particles is insufficient for efficient aggregation or the primary particles are too small to prefer the aggregation process upon collision.

**Table 1.** The characteristic performances of soot generated by different methods. Related references [8,17,36,37,46,59–74].

Property	miniCAST BC Soot					Diesel Soot	Aircraft Soot	Atmospheric Measurement	Spark Discharge GFG1000	Laser Ablation
	Diffusion Flame		Premixed Flame							
	C/O < 0.25	0.25 < C/O < 0.31	C/O < 0.31	C/O < 0.3	C/O < 0.3					
<b>GMD [nm]</b>	≤60–180	180–210	≤40–160	≤30–180	≤40–180	5–20, 30–150	10–50	175.56		
<b>Number concentration [#/cm<sup>3</sup>]</b>	$2 \times 10^5$ – $3 \times 10^7$	$1 \times 10^7$ – $3 \times 10^7$	$1 \times 10^7$ – $5 \times 10^7$	$2 \times 10^6$ – $3 \times 10^7$	$7 \times 10^6$ – $4 \times 10^7$	$10^5$ – $10^9$ – $10^6/10^8$	~ $10^{13}$ – $10^{15}$ #/kg fuel	$6 \times 10^6$	$10^7$	$10^7$
<b>Mass concentration [mg/m<sup>3</sup>]</b>	1–60 eBC (880 nm)	40–180 eBC (880 nm)	0.2–130 eBC (880 nm)	0.1–160 eBC (880 nm)	0.4–150 eBC (880 nm)	0.1–103	0.5–100 mg/kg fuel 20–200 TC	2.6–2.9 µg/m <sup>3</sup> eBC		
<b>Primary particle diameter [nm]</b>			15–45 20–30			16–27	20–50	na	5–7 15–36 5–10	7–13.7
<b>Fractal dimension [–]</b>			2.1–2.2			1.7–2		na	2	1.65–2.1
<b>AAE [–]</b>	≤1.4 ± 0.2	≤1.2 ± 0.1 1.25 (1064–266)	1.1–4.5	1.1–1.7	1.1–4.5	1.1 (450–700 nm) 1.3 1.3 (1064–266) 1.04 (370–950 nm)	–	2.25 (355–1064 nm) 2.23 (370–950) 2 (1064–266) (Winter season) 1.55 (370–950) 1–1.6 (370–950 nm) 1–2.03 (450–660 nm Aethalometer)	2.1 1.8 (1064–266 nm)	1.15 (1064–355 nm) 1.04 (1064–266)
<b>EC/TC [%]</b>	<70–95	<90	2–60	50–95	1–90	60–85	~10–70 80–100	–		

Slightly above this laser fluence (at about  $0.9 \text{ J/cm}^2$ ), the bimodal size distribution has been realized. Here, both primary particles are of around 15 nm size and fractal aggregates with around 100 nm GMD value have appeared. With the further increase of the fluence of the excitation, the fractal aggregates become dominant with a unimodal size distribution comprising GMD and GSD values of about 100 nm and 240 nm, respectively. With the fine tuning of the laser fluences, a defined ratio of spherical primary particles and fractal aggregates can be obtained in this configuration [17]. Even though both the GFG and LA produce soot with unimodal size-distribution of nearly the same GMD values, the LA-produced soot assembly has a greater GSD (Geometric Standard Deviation) value than that of GFG. For example, 20 nm and 600 nm particles can be generated with a yield of about  $10^5$  particles per  $\text{cm}^3$  at  $2 \text{ J/cm}^2$  fluence using  $\text{N}_2$  as purging gas at 200 sccm flow rate [17]. This is critical when bigger particles with high EC content are required for any applications. By increasing the laser fluence or the volumetric flow rate of the purging gas ( $\text{N}_2$ ), it is possible to modify the number-concentration and the GMD value as well. By reducing the flow rate, the CMD value and the number-concentration can be increased. The number concentration increases because at lower flow rates a given volume of the carrier gas resides longer in the ablation chamber, while the emission rate of the produced particles remains constant at a given fluence. The CMD value is increased because at the reduced flow rate the probability of collisions become higher. Using a different mixture of  $\text{N}_2$  and synthetic air as a purging gas, the soot particle evolution can be altered dramatically in a well-controlled manner. Using pure synthetic air as purging gas, the LA soot includes dominant primary particles of spherical geometry. Due to the concomitant oxidation, the generation of fractal aggregates is gradually suppressed by the higher amount of air in the gas mixture. A further and unique advantage of LA approach is that there are no restrictions for target material, as it can be replaced by any real solid fuel target, such as a biomass sample, so the real combustion process, such as biomass or coal burning, can be accurately produced in this configuration [35,36,75]. Compared to the SDG soot, the spectral response of LA soot obtained by using a high purity monolithic graphite sample has imitated the elemental carbon or the freshly emitted diesel soot with high EC content well (Table 1). The AAE value of LA soot is around 1, which fits well to the theoretical expectation for pure elemental carbon [35,37], the experimental measurement of the freshly emitted diesel soot [46], or even the ambient soot aerosol in the summer [36] (Table 1). By changing the target for residential coal originating from different sources of various chemical compositions, different AAE ranging from around 1.3 to 2.5 were realized. The LA technique was used first to demonstrate the source apportionment capabilities of the AAE value for residential coal aerosol from different origins and chemical compositions [35,75]. The LA soot has compact fractal morphology with the fractal dimension and primary particle diameter of about 1.6–2.1 and 7.1 nm to 13.7 nm, respectively. Therefore, considering the morphology and the fractal characteristics of the LA-produced soot, it shows high degree of similarity with real soot or soot-containing aerosol, such as diesel- or biodiesel exhausts [36,37,76]. The structural properties of the primary particles obtained by HR-TEM shows that besides some amorphous and disordered arrangements, the LA soot typically forms in an onion-like (graphitic) molecular structure, where graphene layers are oriented parallel to the external outer surface [17]. This type of microstructure is also in good agreement with that of a more realistic ambient or diesel soot. The recently introduced LA method for the generation of soot particles for environmental applications offers numerous favorable characteristics. One of the major advantages is its green character, namely that it can produce aerosols without or with extremely limited contamination. Although the yield of the LA is smaller than that of SDG, it can produce wider size distributions with relatively high number of both small and large particles. In LA, biomass or other solid fuels can also be used for producing real biomass-combusted soot aerosols under well-controlled measurement conditions. Using Laser-Induced Breakdown Spectroscopy (LIBS), it has been verified experimentally that the LIBS spectra of LA-produced coal aerosols can be used to differentiate the coal aerosols

having different origin [75]. However, one of the major advantages of the LA method is that all the microphysical parameters of the generated soot particles can be tuned independently from each other [17]. This favorable property opens-up novel approaches to investigate the effects of microphysical parameter changes on the measured quantities using the *ceteris paribus* principle.

## 5. Summary and Conclusions

The laser ablation method for the generation of soot aerosol to substitute the carbonaceous particulate matter originating from real combustion is described in the context of its most widely used alternatives in this survey. The evolution of soot in general and under laboratory-controlled conditions using different excitations and fuel types are discussed in detail. The comparative study of the characteristic performances of soot using laser ablation, spark generation, and flame combustion is presented in the context of their application perspectives.

Flames, using fuels with limited chemical compositions and defined gas mixtures make possible to mimic real combustion soot in many physicochemical aspects. In flame chemistry, defined by the C/O ratio, the diverse physicochemical characteristic of soot can be produced, which is a good standard for the real combustion-generated soot associated with fuels and combustion conditions. However, modifying any operational parameters of the burner can lead to changes in some of the microphysical and chemical parameters of the produced aerosol. The independent variation of the characteristic parameters of the generated soot particles cannot be achieved in this configuration. Important applications of flames are to model diesel, kerosene, or real ambient particles, especially in morphology and chemical or optical. The calibration and validation of aerosol measuring instruments with soot standards defined by a specific set of operative conditions of the flame is also an important application area.

The SDG is a simple-to-use instrument for producing carbonaceous aerosols through the spark ablation of a monolithic graphite target. Although significant differences exist between SDG-produced soot and real-world combustion aerosols—especially in terms of chemical composition and molecule structure—its simplicity, stability, and reproducibility make it a useful tool to produce soot aerosol, especially when its physical properties are of primary interest. The size distribution produced by SDG fits well to that of the real combustion-produced carbonaceous aerosols, such as diesel or kerosene soot. Besides the academic applications, one of the major application areas of SDG technique is the calibration of measurement systems used for the characterization of diesel emissions. Since the counting efficiency of calibration material is extremely small and varies from one aerosol standard to another, the inert materials for production of soot standards in an easy and reproducible way is a critical issue for instrument calibration and validation procedures. The SDG equipped with carbon electrodes provide particles with high analytical purity, which allows the production of carbon particles with repeatable morphology in a size domain relevant for diesel emission. Since the counting efficiency of CAST and GFG is very similar for a CPC (condensation particle counter), it can also be applied as an easy-to-use alternative of CAST for instrument calibration as well.

The recently introduced method, based on the laser excitation of high purity graphite material, is a versatile tool for generating soot standards with high similarity to elemental carbon and freshly emitted diesel soot with high EC content. Although the LA and SDG methods differ only in the type of excitation of the graphite target, the characteristic performances of the produced soot aerosol assemblies show some differences. The yield per pulse of LA is smaller than that of SDG. However, the generated soot has a unimodal size distribution of more or less the same GMD values; the GSD values of LA are much higher than that in case of SDG. This allows for the production of relatively high concentrations of particles even in the accumulation mode, which can extend the application area of this approach. Moreover, at low fluences or using synthetic air as purging gas, high number-concentration of primary particles of spherical geometry can be produced. Similarly to the



SDG soot, the LA soot differed significantly from real ambient soot in chemical composition but shows a high degree of similarity in physical characteristics. However, the morphology, the spectral response and the molecular structure of LA soot stands closer to pure elemental carbon or freshly emitted diesel soot than that of the SDG soot. The detailed investigation of Raman spectra has further verified this similarity. Due to the flexibility in the applied target material and purging gas matrix, the LA method opens up novel opportunities for the controlled modeling of biomass emissions too. Finally, a further major advantage of the LA method is that all the physical parameters of the generated soot particles can be tuned independently from one another.

The comparative conclusion of using different generation techniques from an application perspective briefly includes the following: The diffusion flame produces carbonaceous particulate matter with a different and complex set of physicochemical features which imitate real-world combustion soot under laboratory circumstances well. From an application point of view, the diffusion flames are able to produce chemically complex carbonaceous particulate matter, which is closer to the real world combustion aerosol than the soot produced by the SD or LA methods. Therefore, simulating diesel, kerosene, or real ambient aerosol using diffusion flames is more practical for the investigation of OC content effect on the measured quantities. However, during soot evolution, the complex chain reaction of the fuel composite molecules and the degree of contamination of the generated particles limited the applicability of diffusion techniques for being a high-quality aerosol standard for instrument calibration or validation. In the SD and LA methods, the generated soot definitely does not mimic the real world combustion aerosol in its chemical aspects but fits well to its physical characteristics. The SDG is a simple-to-use generator for producing soot aerosol with high EC content primarily for simulate the physical properties of real world combustion particles in the climate-relevant size domain with limited contamination. However, the spectral response of SD soot differs substantially both from the freshly emitted diesel soot and also from the theoretically expected pure elemental or black carbon particles. Despite those limitations, both the diffusion flames and also the SD technique are widely used for producing aerosol standards for instrument calibration or validation. The recently introduced LA technique, based on the precisely controlled laser excitation of solid fuel target, produces a high-quality contamination-free soot aerosol standard with high EC content for the simulation of the freshly emitted diesel soot or real ambient BC aerosol, especially when the physical properties are of concern. The spectral property of LA-produced soot is closer to real world combustion BC, such as freshly emitted diesel or ambient BC, than that of the SD-generated particles. Moreover, the LA technique is more flexible regarding applied fuel than the SD method. Real combustion particles using real biomass or coal samples can also be produced under well-controlled combustion conditions with LA. In contrast to diffusion flames or the SD technique, LA is capable of producing real combustion carbonaceous aerosol under well-controlled laboratory circumstances using solid fuel target. In comparison, from an application point of view, one of the biggest advantages of the LA technique is that all microphysical parameters of the generated soot particles can be varied independently from each other, which opens up a novel opportunity to investigate defined physical quantities of the generated soot using the *ceteris paribus* principle. A practical example is the potential to decrease the uncertainty associated with source apportionment methods [77,78].

**Author Contributions:** Conceptualization, T.A., A.K., P.R., G.S. and Z.B.; Methodology, T.A., A.K., P.R., G.S. and Z.B.; Writing—original draft, T.A. All authors have read and agreed to the published version of the manuscript.

**Funding:** This work was supported by the Materials science and photonics TKP 2021 (project ITM NKFIA TKP2021-NVA-19). One of the authors (A. Kohut) is also grateful for the Ministry of Innovation and Technology of Hungary for the funding provided from the National Research, Development and Innovation Fund under the PD\_21 OTKA funding scheme (PD 139077 project).

**Institutional Review Board Statement:** Not applicable.

**Informed Consent Statement:** Not applicable.

**Data Availability Statement:** Not applicable.

**Conflicts of Interest:** The authors declare no conflict of interest.

## References

1. Lohmann, U.; Friebel, F.; Kanji, Z.A.; Mahrt, F.; Mensah, A.A.; Neubauer, D. Future Warming Exacerbated by Aged-Soot Effect on Cloud Formation. *Nat. Geosci.* **2020**, *13*, 674–680. [[CrossRef](#)]
2. Bond, T.C.; Doherty, S.J.; Fahey, D.W.; Forster, P.M.; Berntsen, T.; Deangelo, B.J.; Flanner, M.G.; Ghan, S.; Kärcher, B.; Koch, D.; et al. Bounding the Role of Black Carbon in the Climate System: A Scientific Assessment. *J. Geophys. Res. Atmos.* **2013**, *118*, 5380–5552. [[CrossRef](#)]
3. Liu, P.; Kaplan, J.O.; Mickley, L.J.; Li, Y.; Chellman, N.J.; Arienzo, M.M.; Kodros, J.K.; Pierce, J.R.; Sigl, M.; Freitag, J.; et al. Improved Estimates of Preindustrial Biomass Burning Reduce the Magnitude of Aerosol Climate Forcing in the Southern Hemisphere. *Sci. Adv.* **2021**, *7*, eabc1379. [[CrossRef](#)]
4. Costa, D.L. Historical Highlights of Air Pollution Toxicology. *Toxicol. Sci.* **2018**, *164*, 5–8. [[CrossRef](#)] [[PubMed](#)]
5. Zhao, F.; Yang, W.; Yu, W. A Progress Review of Practical Soot Modelling Development in Diesel Engine Combustion. *J. Traffic Transp. Eng. Engl. Ed.* **2020**, *7*, 269–281. [[CrossRef](#)]
6. Dockery, D.W.; Pope, C.A., III; Xu, X.; Spengler, J.D.; Ware, J.H.; Fay, M.E.; Ferris, B.G.; Speizer, F.E. An association between air pollution and mortality in six U.S. cities. *N. Engl. J. Med.* **1993**, *329*, 1753–1759. [[CrossRef](#)]
7. Martin, J.W.; Salamanca, M.; Kraft, M. Soot Inception: Carbonaceous Nanoparticle Formation in Flames. *Prog. Energy Combust. Sci.* **2022**, *88*, 100956. [[CrossRef](#)]
8. Ajtai, T.; Kiss-Albert, G.; Utry, N.; Tóth, Á.; Hoffer, A.; Szabó, G.; Bozóki, Z. Diurnal Variation of Aethalometer Correction Factors and Optical Absorption Assessment of Nucleation Events Using Multi-Wavelength Photoacoustic Spectroscopy. *J. Environ. Sci. China* **2019**, *83*, 96–109. [[CrossRef](#)]
9. Petzold, A.; Ogren, J.A.; Fiebig, M.; Laj, P.; Li, S.M.; Baltensperger, U.; Holzer-Popp, T.; Kinne, S.; Pappalardo, G.; Sugimoto, N.; et al. Recommendations for Reporting Black Carbon Measurements. *Atmos. Chem. Phys.* **2013**, *13*, 8365–8379. [[CrossRef](#)]
10. Andreae, M.O.; Gelencsér, A. Black Carbon or Brown Carbon? The Nature of Light-Absorbing Carbonaceous Aerosols. *Atmos. Chem. Phys.* **2006**, *6*, 3131–3148. [[CrossRef](#)]
11. Török, S.; Malmberg, V.B.; Simonsson, J.; Eriksson, A.; Martinsson, J.; Mannazhi, M.; Pagels, J.; Bengtsson, P.E. Investigation of the Absorption Ångström Exponent and Its Relation to Physicochemical Properties for Mini-CAST Soot. *Aerosol Sci. Technol.* **2018**, *52*, 757–767. [[CrossRef](#)]
12. Ess, M.N.; Vasilatou, K. Characterization of a New MiniCAST with Diffusion Flame and Premixed Flame Options: Generation of Particles with High EC Content in the Size Range 30 Nm to 200 Nm. *Aerosol Sci. Technol.* **2019**, *53*, 29–44. [[CrossRef](#)]
13. Mason, Y.C.; Schoonraad, G.L.; Orasche, J.; Bisig, C.; Jakobi, G.; Zimmermann, R.; Forbes, P.B.C. Comparative Sampling of Gas Phase Volatile and Semi-Volatile Organic Fuel Emissions from a Combustion Aerosol Standard System. *Environ. Technol. Innov.* **2020**, *19*, 100945. [[CrossRef](#)]
14. Hagen, F.P.; Rinkenburger, A.; Günther, J.; Bockhorn, H.; Niessner, R.; Suntz, R.; Loukou, A.; Trimis, D.; Haisch, C. Spark Discharge-Generated Soot: Varying Nanostructure and Reactivity against Oxidation with Molecular Oxygen by Synthesis Conditions. *J. Aerosol Sci.* **2020**, *143*, 105530. [[CrossRef](#)]
15. Bischof, O.F.; Weber, P.; Bundke, U.; Petzold, A.; Kiendler-Scharr, A. Characterization of the Miniaturized Inverted Flame Burner as a Combustion Source to Generate a Nanoparticle Calibration Aerosol. *Emiss. Control. Sci. Technol.* **2020**, *6*, 37–46. [[CrossRef](#)]
16. Haller, T.; Rentenberger, C.; Meyer, J.C.; Felgitsch, L.; Grothe, H.; Hitzenberger, R. Structural Changes of CAST Soot during a Thermal-Optical Measurement Protocol. *Atmos. Meas. Tech.* **2019**, *12*, 3503–3519. [[CrossRef](#)]
17. Ajtai, T.; Utry, N.; Pintér, M.; Kiss-Albert, G.; Puskás, R.; Tápai, C.; Kecskeméti, G.; Smausz, T.; Hopp, B.; Bozóki, Z.; et al. Microphysical Properties of Carbonaceous Aerosol Particles Generated by Laser Ablation of a Graphite Target. *Atmos. Meas. Tech.* **2015**, *8*, 1207–1215. [[CrossRef](#)]
18. Preining, O.D.E.J.; der, W.Ö.A. (Eds.) *History of Aerosol Science: Proceedings of Symposium on the History of Aerosol Science Held in Vienna*; Österreichische Akademie der Wissenschaften: Vienna, Austria, 2000.
19. Faccineto, A.; Irimiea, C.; Minutolo, P.; Commodo, M.; D’anna, A.; Nuns, N.; Carpentier, Y.; Pirim, C.; Desgroux, P.; Focsa, C.; et al. Evidence on the formation of dimers of polycyclic aromatic hydrocarbons in a laminar diffusion flame. *Commun. Chem.* **2020**, *3*, 112. [[CrossRef](#)]
20. Sabbah, H.; Commodo, M.; Picca, F.; De Falco, G.; Minutolo, P.; D’Anna, A.; Joblin, C. Molecular content of nascent soot: Family characterization using two-step laser desorption laser ionization mass spectrometry. *Proc. Combust. Inst.* **2021**, *38*, 1241–1248. [[CrossRef](#)]
21. Michelsen, H.A. Effects of maturity and temperature on soot density and specific heat. *Proc. Combust. Inst.* **2021**, *38*, 1197–1205. [[CrossRef](#)]

22. Liu, C.; Singh, A.V.; Saggese, C.; Tang, Q.; Chen, D.; Wan, K.; Vinciguerra, M.; Comodo, M.; De Falco, G.; Minutolo, P.; et al. Flame-formed carbon nanoparticles exhibit quantum dot behaviors. *Proc. Natl. Acad. Sci. USA* **2019**, *116*, 12692–12697. [[CrossRef](#)] [[PubMed](#)]
23. Constantine, M.M.; Richard, A.D. Comparison of soot growth and oxidation in smoking and non-smoking ethylene diffusion flames. *Combust. Sci. Technol.* **1989**, *66*, 1–16. [[CrossRef](#)]
24. Helsper, C.; Mölter, W.; Löffler, F.; Wadenpohl, C.; Kaufmann, S.; Wenninger, G. Investigations of a New Aerosol Generator for the Production of Carbon Aggregate Particles. *Atmos. Environ. Part A Gen. Top.* **1993**, *27*, 1271–1275. [[CrossRef](#)]
25. Baumgardner, D.; Popovicheva, O.; Allan, J.; Bernardoni, V.; Cao, J.; Cavalli, F.; Cozic, J.; Diapouli, E.; Eleftheriadis, K.; Genberg, P.J.; et al. Soot Reference Materials for Instrument Calibration and Intercomparisons: A Workshop Summary with Recommendations. *Atmos. Meas. Tech.* **2012**, *5*, 1869–1887. [[CrossRef](#)]
26. Kohut, A.; Ludvigsson, L.; Meuller, B.O.; Deppert, K.; Messing, M.E.; Galbács, G.; Geretovszky, Z. From Plasma to Nanoparticles: Optical and Particle Emission of a Spark Discharge Generator. *Nanotechnology* **2017**, *28*, 475603. [[CrossRef](#)]
27. Feng, J.; Huang, L.; Ludvigsson, L.; Messing, M.E.; Maisser, A.; Biskos, G.; Schmidt-Ott, A. General Approach to the Evolution of Singlet Nanoparticles from a Rapidly Quenched Point Source. *J. Phys. Chem. C* **2016**, *120*, 621–630. [[CrossRef](#)]
28. Hakjoo, K.; Jinho, K.; Youngjoo, C.; Hyenchul, O.; Jungbum, C.; Sangsoo, K. Generation of Model Diesel Particles by Spark Discharge and Hydrocarbon Condensation. *J. Mech. Sci. Technol.* **2006**, *20*, 1972–1979. [[CrossRef](#)]
29. Roth, C.; Ferron, G.A.; Karg, E.; Lentner, B.; Schumann, G.; Takenaka, S.; Heyder, J. Generation of Ultrafine Particles by Spark Discharging. *Aerosol Sci. Technol.* **2010**, *38*, 228–235. [[CrossRef](#)]
30. Itina, T.E.; Voloshko, A. Nanoparticle Formation by Laser Ablation in Air and by Spark Discharges at Atmospheric Pressure. *Appl. Phys. B Lasers Opt.* **2013**, *113*, 473–478. [[CrossRef](#)]
31. Garrison, B.J.; Itina, T.E.; Zhigilei, L.V. Limit of Overheating and the Threshold Behavior in Laser Ablation. *Phys. Rev. E* **2003**, *68*, 041501. [[CrossRef](#)]
32. Vidal, F.; Johnston, T.W.; Laville, S.; Barthélemy, O.; Chaker, M.; le Drogoff, B.; Margot, J.; Sabsabi, M. Critical-Point Phase Separation in Laser Ablation of Conductors. *Phys. Rev. Lett.* **2001**, *86*, 2573. [[CrossRef](#)] [[PubMed](#)]
33. Raizer, Y.P. *Gas Discharge Physics*; Springer: Berlin/Heidelberg, Germany, 1991. [[CrossRef](#)]
34. Kohut, A.; Galbács, G.; Márton, Z.; Geretovszky, Z. Characterization of a Copper Spark Discharge Plasma in Argon Atmosphere Used for Nanoparticle Generation. *Plasma Sources Sci. Technol.* **2017**, *26*, 045001. [[CrossRef](#)]
35. Pintér, M.; Ajtai, T.; Kiss-Albert, G.; Utry, N.; Kiss, D.; Smausz, T.; Kohut, A.; Hopp, B.; Galbács, G.; Kukovecz, Á.; et al. Thermo-Optical Properties of Residential Coals and Combustion Aerosols. *Atmos. Environ.* **2018**, *178*, 118–128. [[CrossRef](#)]
36. Utry, N.; Ajtai, T.; Pintér, M.; Bozóki, Z.; Szabó, G. Wavelength-Dependent Optical Absorption Properties of Artificial and Atmospheric Aerosol Measured by a Multi-Wavelength Photoacoustic Spectrometer. *Int. J. Thermophys.* **2014**, *35*, 2246–2258. [[CrossRef](#)]
37. Ajtai, T.; Filep, Á.; Kecskeméti, G.; Hopp, B.; Bozóki, Z.; Szabó, G.; Ajtai, T.; Filep, Á.; Kecskeméti, G.; Szabó, G.; et al. Wavelength Dependent Mass-Specific Optical Absorption Coefficients of Laser Generated Coal Aerosols Determined from Multi-Wavelength Photoacoustic Measurements. *Appl. Phys. A* **2010**, *103*, 1165–1172. [[CrossRef](#)]
38. Bockhorn, H. (Ed.) *Soot Formation in Combustion*; Springer: Berlin/Heidelberg, Germany, 1994. [[CrossRef](#)]
39. Bockhorn, H.; D’Anna, A.; Sarofim, A.F.; Wang, H. (Eds.) *Combustion Generated Fine Carbonaceous Particles*; Universitätsverlag Karlsruhe: Karlsruhe, Germany, 2009.
40. Xi, J.; Yang, G.; Cai, J.; Gu, Z. A Review of Recent Research Results on Soot: The Formation of a Kind of Carbon-Based Material in Flames. *Front. Mater.* **2021**, *8*, 179. [[CrossRef](#)]
41. Wang, Y.; Chung, S.H. Soot formation in laminar counterflow flames. *Prog. Energy Combust. Sci.* **2019**, *74*, 152–238. [[CrossRef](#)]
42. Wang, W.; Zhang, Z.; Shi, D.; Huang, Y.; Zhou, L. Study of soot formations in co-flow laminar diffusion flames of n-heptane and oxygenated aromatic biofuels from atmospheric condition to 2.3 bar. *Fuel* **2021**, *297*, 120753. [[CrossRef](#)]
43. Sun, Z.; Dally, B.; Alwahabi, Z.; Nathan, G. The effect of oxygen concentration in the co-flow of laminar ethylene diffusion flames. *Combust. Flame* **2020**, *211*, 96–111. [[CrossRef](#)]
44. Horvath, H.; Gangl, M. A Low-Voltage Spark Generator for Production of Carbon Particles. *J. Aerosol Sci.* **2003**, *34*, 1581–1588. [[CrossRef](#)]
45. Feng, J.; Hontañón, E.; Blanes, M.; Meyer, J.; Guo, X.; Santos, L.; Paltrinieri, L.; Ramlawi, N.; Smet, L.C.P.M.D.; Nirschl, H.; et al. Scalable and Environmentally Benign Process for Smart Textile Nanofinishing. *ACS Appl. Mater. Interfaces* **2016**, *8*, 14756–14765. [[CrossRef](#)] [[PubMed](#)]
46. Schnaiter, M.; Horvath, H.; Möhler, O.; Naumann, K.H.; Saathoff, H.; Schöck, O.W. UV-VIS-NIR Spectral Optical Properties of Soot and Soot-Containing Aerosols. *J. Aerosol Sci.* **2003**, *34*, 1421–1444. [[CrossRef](#)]
47. You, R.; Radney, J.G.; Zachariah, M.R.; Zangmeister, C.D. Measured Wavelength-Dependent Absorption Enhancement of Internally Mixed Black Carbon with Absorbing and Nonabsorbing Materials. *Environ. Sci. Technol.* **2016**, *50*, 7982–7990. [[CrossRef](#)]
48. Horender, S.; Auderset, K.; Vasilatou, K. Facility for Calibration of Optical and Condensation Particle Counters Based on a Turbulent Aerosol Mixing Tube and a Reference Optical Particle Counter. *Rev. Sci. Instrum.* **2019**, *90*, 075111. [[CrossRef](#)] [[PubMed](#)]
49. Moosmüller, H.; Chakrabarty, R.K.; Arnott, W.P. Aerosol Light Absorption and Its Measurement: A Review. *J. Quant. Spectrosc. Radiat. Transf.* **2009**, *110*, 844–878. [[CrossRef](#)]

50. Bescond, A.; Yon, J.; Ouf, F.X.; Rozé, C.; Coppalle, A.; Parent, P.; Ferry, D.; Laffon, C. Soot Optical Properties Determined by Analyzing Extinction Spectra in the Visible Near-UV: Toward an Optical Speciation According to Constituents and Structure. *J. Aerosol Sci.* **2016**, *101*, 118–132. [[CrossRef](#)]
51. Lefevre, G.; Yon, J.; Liu, F.; Coppalle, A. Spectrally Resolved Light Extinction Enhancement of Coated Soot Particles. *Atmos. Environ.* **2018**, *186*, 89–101. [[CrossRef](#)]
52. Malmborg, V.; Eriksson, A.; Gren, L.; Török, S.; Shamun, S.; Novakovic, M.; Zhang, Y.; Kook, S.; Tunér, M.; Bengtsson, P.E.; et al. Characteristics of BrC and BC Emissions from Controlled Diffusion Flame and Diesel Engine Combustion. *Aerosol Sci. Technol.* **2021**, *55*, 769–784. [[CrossRef](#)]
53. Ess, M.N.; Bertò, M.; Irwin, M.; Modini, R.L.; Gysel-Beer, M.; Vasilatou, K. Optical and Morphological Properties of Soot Particles Generated by the MiniCAST 5201 BC Generator. *Aerosol Sci. Technol.* **2021**, *55*, 828–847. [[CrossRef](#)]
54. Byeon, J.H.; Park, J.H.; Yoon, K.Y.; Ko, B.J.; Ji, J.H.; Hwang, J. Removal of Volatile Organic Compounds by Spark Generated Carbon Aerosol Particles. *Carbon* **2006**, *44*, 2106–2108. [[CrossRef](#)]
55. Chae, S.; Lee, D.; Kim, M.C.; Kim, D.S.; Choi, M. Wire-in-Hole-Type Spark Discharge Generator for Long-Time Consistent Generation of Unagglomerated Nanoparticles. *Aerosol Sci. Technol.* **2015**, *49*, 463–471. [[CrossRef](#)]
56. Alfè, M.; Gargiulo, V.; de Luca, O.; Rudolf, P.; Zhang, B.; Sabia, P.; de Joannon, M. Easy tuning of nanotexture and N doping of carbonaceous particles produced by spark discharge. *Carbon Trends* **2021**, *5*, 100134. [[CrossRef](#)]
57. Burtscher, H. Application of a Spark Discharge Generator for Production of Combustion-Like Aerosols. In *Spark Ablation*; Jenny Stanford Publishing: Dubai, United Arab Emirates, 2020; pp. 421–445. [[CrossRef](#)]
58. Jeong, B.; Lee, J. Effective Density and Light Absorption Cross Section of Black Carbon Generated in a Spark Discharger. *J. Aerosol Sci.* **2017**, *107*, 55–64. [[CrossRef](#)]
59. An, P.; Sun, W.; Li, G.; Tan, M.; Lai, C.; Chen, S. Characteristics of Particle Size Distributions About Emissions in A Common-Rail Diesel Engine with Biodiesel Blends. *Procedia Environ. Sci.* **2011**, *11*, 1371–1378. [[CrossRef](#)]
60. Ess, M.N.; Blatt, H.; Mühlbauer, W.; Seher, S.I.; Zöllner, C.; Lorenz, S.; Brüggemann, D.; Nieken, U.; Ivleva, N.P.; Niessner, R. Reactivity and Structure of Soot Generated at Varying Biofuel Content and Engine Operating Parameters. *Combust. Flame* **2016**, *163*, 157–169. [[CrossRef](#)]
61. Caroca, J.C.; Millo, F.; Veza, D.; Vlachos, T.; de Filippo, A.; Bensaid, S.; Russo, N.; Fino, D. Detailed Investigation on Soot Particle Size Distribution during DPF Regeneration, Using Standard and Bio-Diesel Fuels. *Ind. Eng. Chem. Res.* **2011**, *50*, 2650–2658. [[CrossRef](#)]
62. Kittelson, D.B. Engines and Nanoparticles: A Review. *J. Aerosol Sci.* **1998**, *29*, 575–588. [[CrossRef](#)]
63. Lu, T.; Huang, Z.; Cheung, C.S.; Ma, J. Size Distribution of EC, OC and Particle-Phase PAHs Emissions from a Diesel Engine Fueled with Three Fuels. *Sci. Total Environ.* **2012**, *438*, 33–41. [[CrossRef](#)]
64. Abegglen, M.; Brem, B.T.; Ellenrieder, M.; Durdina, L.; Rindlisbacher, T.; Wang, J.; Lohmann, U.; Sierau, B. Chemical Characterization of Freshly Emitted Particulate Matter from Aircraft Exhaust Using Single Particle Mass Spectrometry. *Atmos. Environ.* **2016**, *134*, 181–197. [[CrossRef](#)]
65. Lobo, P.; Durdina, L.; Smallwood, G.J.; Rindlisbacher, T.; Siegerist, F.; Black, E.A.; Yu, Z.; Mensah, A.A.; Hagen, D.E.; Miake-Lye, R.C.; et al. Measurement of Aircraft Engine Non-Volatile PM Emissions: Results of the Aviation-Particle Regulatory Instrumentation Demonstration Experiment (A-PRIDE) 4 Campaign. *Aerosol Sci. Technol.* **2015**, *49*, 472–484. [[CrossRef](#)]
66. Popovitcheva, O.B.; Persiantseva, N.M.; Trukhin, M.E.; Rulev, G.B.; Shonija, N.K.; Buriko, Y.Y.; Starik, A.M.; Demirdjian, B.; Ferry, D.; Suzanne, J. Experimental Characterization of Aircraft Combustor Soot: Microstructure, Surface Area, Porosity and Water Adsorption. *Phys. Chem. Chem. Phys.* **2000**, *2*, 4421–4426. [[CrossRef](#)]
67. Durdina, L.; Lobo, P.; Trueblood, M.B.; Black, E.A.; Achterberg, S.; Hagen, D.E.; Brem, B.T.; Wang, J. Response of Real-Time Black Carbon Mass Instruments to Mini-CAST Soot. *Aerosol Sci. Technol.* **2016**, *50*, 906–918. [[CrossRef](#)]
68. Cheng, M.D.; Corporan, E.; Dewitt, M.J.; Landgraf, B. Emissions of Volatile Particulate Components from Turboshift Engines Operated with JP-8 and Fischer-Tropsch Fuels. *Aerosol Air Qual. Res.* **2009**, *9*, 237–256. [[CrossRef](#)]
69. Zangmeister, C.D.; You, R.; Lunny, E.M.; Jacobson, A.E.; Okumura, M.; Zachariah, M.R.; Radney, J.G. Measured In-Situ Mass Absorption Spectra for Nine Forms of Highly-Absorbing Carbonaceous Aerosol. *Carbon* **2018**, *136*, 85–93. [[CrossRef](#)]
70. Drinovec, L.; Gregoric, A.; Zotter, P.; Wolf, R.; Anne Bruns, E.; Bruns, E.A.; Prevot, A.S.H.; Favez, O.; Sciare, J.; Arnold, I.J.; et al. The Filter-Loading Effect by Ambient Aerosols in Filter Absorption Photometers Depends on the Coating of the Sampled Particles. *Atmos. Meas. Tech.* **2017**, *10*, 1043–1059. [[CrossRef](#)]
71. Zhang, G.; Peng, L.; Lian, X.; Lin, Q.; Bi, X.; Chen, D.; Li, M.; Li, L.; Wang, X.; Sheng, G. An Improved Absorption Ångström Exponent (AAE)-Based Method for Evaluating the Contribution of Light Absorption from Brown Carbon with a High-Time Resolution. *Aerosol Air Qual. Res.* **2019**, *19*, 15–24. [[CrossRef](#)]
72. Costabile, F.; Alas, H.; Aufderheide, M.; Avino, P.; Amato, F.; Argentini, S.; Barnaba, F.; Berico, M.; Bernardoni, V.; Biondi, R.; et al. First Results of the “Carbonaceous Aerosol in Rome and Environs (CARE)” Experiment: Beyond Current Standards for PM10. *Atmosphere* **2017**, *8*, 249. [[CrossRef](#)]
73. Moore, R.H.; Ziemba, L.D.; Dutcher, D.; Beyersdorf, A.J.; Chan, K.; Crumeyrolle, S.; Raymond, T.M.; Thornhill, K.L.; Winstead, E.L.; Anderson, B.E. Mapping the Operation of the Miniature Combustion Aerosol Standard (Mini-CAST) Soot Generator. *Aerosol Sci. Technol.* **2014**, *48*, 467–479. [[CrossRef](#)]



74. Kuznetsov, B.v.; Rakhmanova, T.A.; Popovicheva, O.B.; Shonija, N.K. Water Adsorption and Energetic Properties of Spark Discharge Soot: Specific Features of Hydrophilicity. *J. Aerosol Sci.* **2003**, *34*, 1465–1479. [[CrossRef](#)]
75. Palásti, D.J.; Metzinger, A.; Ajtai, T.; Bozóki, Z.; Hopp, B.; Kovács-Széles, E.; Galbács, G. Qualitative Discrimination of Coal Aerosols by Using the Statistical Evaluation of Laser-Induced Breakdown Spectroscopy Data. *Spectrochim. Acta Part B At. Spectrosc.* **2019**, *153*, 34–41. [[CrossRef](#)]
76. Tumolva, L.; Park, J.Y.; Kim, J.S.; Miller, A.L.; Chow, J.C.; Watson, J.G.; Park, K. Morphological and Elemental Classification of Freshly Emitted Soot Particles and Atmospheric Ultrafine Particles Using the TEM/EDS. *Aerosol Sci. Technol.* **2010**, *44*, 202–215. [[CrossRef](#)]
77. Utry, N.; Ajtai, T.; Filep, Á.; Pintér, M.; Török, Z.; Bozóki, Z.; Szabó, G. Correlations between Absorption Angström Exponent (AAE) of Wintertime Ambient Urban Aerosol and Its Physical and Chemical Properties. *Atmos. Environ.* **2014**, *91*, 52–59. [[CrossRef](#)]
78. Ajtai, T.; Utry, N.; Pintér, M.; Major, B.; Bozóki, Z.; Szabó, G. A Method for Segregating the Optical Absorption Properties and the Mass Concentration of Winter Time Urban Aerosol. *Atmos. Environ.* **2015**, *122*, 313–320. [[CrossRef](#)]